American Mineralogist, Volume 107, pages 1164–1173, 2022

Gungerite, $TlAs_5Sb_4S_{13}$, a new thallium sulfosalt with a complex structure containing covalent As-As bonds

Anatoly V. Kasatkin[1], Jakub Plášil[2,*], Emil Makovicky[3], Nikita V. Chukanov[4], Radek Škoda[5], Atali A. Agakhanov[1], and Mikhail V. Tsyganko[6]

[1]Fersman Mineralogical Museum of the Russian Academy of Sciences, Leninsky Prospekt 18-2, 119071 Moscow, Russia
[2]Institute of Physics ASCR, v.v.i., Na Slovance 1999/2, 18221 Prague 8, Czech Republic
[3]Department of Geoscience and Resource Management, University of Copenhagen, Østervoldgade 10, DK-1350, Copenhagen K, Denmark
[4]Institute of Problems of Chemical Physics, Russian Academy of Sciences, Chernogolovka, 142432, Moscow Region, Russia
[5]Department of Geological Sciences, Faculty of Science, Masaryk University, Kotlářská 2, 611 37, Brno, Czech Republic
[6]40 Let Oktyabrya street 15, Kalya, Severouralsk, Sverdlovskaya Oblast', 624474 Russia

Abstract

Gungerite, $TlAs_5Sb_4S_{13}$, is a new mineral from the Vorontsovskoye gold deposit in Northern Urals. It occurs in limestone breccias composed of calcite and dolomite and cemented by orpiment, pyrite, realgar, stibnite, and minor baryte and quartz. It belongs to the latest phases among sulfosalts (chiefly Tl-As-Sb ones) present in the ore. The empirical formula (based on the sum of all atoms = 23 pfu) is $Tl_{0.99}As_{5.29}Sb_{3.77}S_{12.95}$. The Raman spectrum exhibits bands corresponding to As-S and Sb-S stretching vibrations, and a band at 263 cm^{-1} that is assigned to As–As stretching vibrations. Gungerite is bright orange with an orange streak, greasy luster, and perfect cleavage on {010}. It is translucent in thin fragments. The calculated density is 4.173 g/cm^3. In reflected light, the mineral is yellowish-white with very weak bireflectance. In crossed polars, it is distinctly anisotropic but anisotropy effects are masked by strong internal reflections of bright orange color. Gungerite is orthorhombic, with the space group *Pbcn*. Unit-cell parameters determined from the single-crystal X-ray diffraction data are as follows: a = 20.1958(3) Å, b = 11.5258(2) Å, c = 20.1430(2) Å, and V = 4688.74(12) $Å^3$ (Z = 8). The crystal structure consists of doughnut-shaped (As,Sb)-S clusters, which have van der Waals contacts to most of the surroundings, and are connected to them only by sparse cation-sulfur bonds. These clusters are formed by a chelating mirror-symmetrical group, which is "stacked" on, around, and along rods of the TlS_9 coordination polyhedra; these rods are oriented parallel to [010]. An individual doughnut-shaped cluster with a central TlS_9 polyhedron half-inserted into it contains one As–As bond 2.449 Å long. The polar Tl rods form a chessboard arrangement with occasional stacking errors leading to twinning on (101). The large and complex structure of gungerite shows remote similarities to that of gillulyite and the rod-like structure of lorándite.

Keywords: Gungerite, new mineral species, Tl-As-Sb sulfosalt, Raman spectroscopy, crystal structure, covalent bonds; Vorontsovskoe gold deposit

Introduction

Thallium and its compounds play a very important role in a wide variety of industrial applications (Gresham and Lawrey 2018; https://www.usgs.gov/centers/nmic/thallium-statistics-and-information): they are applied in the manufacture of electronic devices, optical lenses with a high-refractive index, semiconductor materials, alloys, γ radiation detection equipment, infrared radiation detection and transmission equipment, crystalline filters for light diffraction for acoustic-optical measuring devices, low-temperature thermometers, in the synthesis of organic compounds, and in a high-density liquid for sink-float separation of minerals. Also, research activity with thallium is ongoing to develop high-temperature superconducting materials for such applications as magnetic resonance imaging, storage of magnetic energy, magnetic propulsion, and electric power generation and transmission. Trace amounts of thallium are used as a contrast agent in the visualization of cardiac function and tumors. On the other hand, thallium compounds show a very strong level of toxicity and should be strictly controlled to prevent harm to humans and the environment. Although thallium is moderately abundant in the Earth's crust [for instance, the average content of Tl in granites is 1.5 ppm (Turekian and Wedepohl 1961)], it is mostly dispersed in association with potassium minerals in clays, granites, and soils, and is not generally considered to be commercially recoverable from those materials. The major sources of recoverable thallium are gold and complex sulfide ores (Ikramuddin 1985; Karbowska 2016). Because of the above, much attention of geologists and mineralogists is given to the research of gold deposits that bear Tl-mineralization and to the study of new Tl-bearing mineral species and their structures.

Herein, we describe the new sulfosalt mineral gungerite

* E-mail: jakub.horrak@gmail.com. Orcid 0000-0001-6627-5742

0003-004X/22/0006–1164$05.00/DOI: https://doi.org/10.2138/am-2022-8003

containing thallium as a species-defining element. Gungerite was found at the Vorontsovskoe gold deposit located in the Northern Urals, Russia. This deposit is unique with regard to the diversity and originality of its Tl-Hg-Mn-As-Sb-S mineralization, where gungerite is a remarkable example of a sulfosalt having complicated complex crystal structure both with covalent and van der Waals bonds. Its name honors Yuri Vladimirovich Gunger (born August 6, 1961), a mining engineer and surveyor, famous historian, and expert of Northern Urals. Both the name and the new mineral were approved by the Commission on New Minerals, Nomenclature and Classification of the International Mineralogical Association (the proposal IMA2020-009). The holotype specimen is deposited in the collections of the Fersman Mineralogical Museum of the Russian Academy of Sciences, Moscow, Russia, with registration number 5518/1.

Occurrence

Specimens containing the new mineral were collected in March 2016 at the main ore stockpile of the Vorontsovskoe gold deposit, approximately 13 km to the south of the city of Krasnotur'insk, Sverdlovskaya Oblast', Northern Urals, Russia (59°38′50″N, 60°12′52″E). A detailed description of the deposit, its genesis, geology, and composition of main types of ores can be found elsewhere (Sazonov et al. 1998; Vikentyev et al. 2016; Murzin et al. 2017; Kasatkin et al. 2018a, 2018b, 2019, 2020). Kasatkin et al. (2022a) recently summarized the history of the study of the deposit and its geological background, provided the description of main mineral assemblages, and 210 mineral species identified there. Among them, eight are new minerals discovered by our team and all of them are sulfosalts: vorontsovite, ferrovorontsovite (Kasatkin et al. 2018a), tsygankoite (Kasatkin et al. 2018b), gladkovskyite (Kasatkin et al. 2019), luboržákite (Kasatkin et al. 2020), pokhodyashinite (Kasatkin et al. 2022b), auerbakhite (Kasatkin et al. 2021), and gungerite described herein.

Gungerite was found in carbonate breccias composed mainly of calcite and dolomite and cemented by orpiment, pyrite, realgar, stibnite, and minor baryte and quartz. Other associated minerals include bernardite, minerals of chabournéite-dalnegroite and vorontsovite–ferrovorontsovite series, cinnabar, coloradoite, gold, greigite, hutchinsonite, parapierrotite, and routhierite. Most likely, gungerite was formed in the latest stage of the low-temperature hydrothermal process.

Physical properties

Among all the new minerals discovered at the Vorontsovskoe deposit, gungerite is the only one that forms macroscopic segregations visible by the naked eye: its fine-grained aggregates fill areas up to 0.5 × 0.2 cm on the surface of carbonate breccias (Figs. 1 and 2). It has a bright orange color, orange streak and greasy luster. Gungerite is translucent in thin fragments, brittle, and has an uneven fracture. Perfect cleavage on {010} has been observed. The new mineral does not exhibit any fluorescence under UV radiation. The Vickers hardness (VHN, 10 g load) is 84 kg/mm^2 (range 74–98 kg/mm^2, n = 4), corresponding to a Mohs hardness of 2–2½. The density of gungerite could not be measured because of the absence of suitable heavy liquids. The density calculated based on the empirical formula (Z = 8) and the unit-cell volume determined from the single-crystal X-ray diffraction data is 4.173 g/cm^3. In reflected light, gungerite is yellowish-white, but at contact with stibnite it looks light gray with a weak bluish tint. Bireflectance is very weak. The new mineral is distinctly anisotropic, but anisotropy effects are masked by internal reflections of bright orange color. The latter is seen even in one nicol, while in crossed polars in air and especially in immersion they are extremely abundant and strong. Quantitative reflectance measurements were performed in the air relative to a WTiC standard using a Universal Microspectrophotometer UMSP 50 (Opton-Zeiss, Germany). Reflectance values are given in Table 1.

Figure 1. Orange fine-grained aggregates of gungerite in carbonate breccia with black powdery greigite. Size of the sample: 5 × 4 cm. Photo: A.D. Kasatkina.

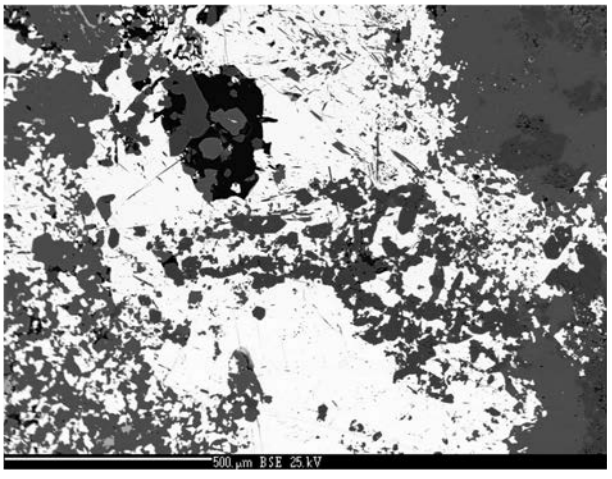

Figure 2. Massive aggregates of gungerite (white) in calcite (medium gray) and quartz (dark gray) matrix. Polished section, SEM (BSE) image.

Raman spectroscopy

The Raman spectrum of gungerite (Fig. 3) was obtained from the polished section utilizing a Horiba Labram HR Evolution spectrometer. This dispersive, edge-filter-based system is equipped with an Olympus BX 41 optical microscope, a diffraction grating with 600 grooves per millimeter, and a Peltier-cooled,

Table 1. Reflectance values of gungerite (in percentages)

λ (nm)	R_1	R_2	λ (nm)	R_1	R_2
400	33.3	27.8	560	27.0	25.7
420	31.1	27.7	580	26.2	25.1
440	30.1	26.5	**589**	**25.9**	**24.5**
460	29.8	26.7	600	25.6	24.0
470	**29.8**	**27.0**	620	24.9	23.5
480	29.9	27.3	640	24.2	22.8
500	29.4	27.4	**650**	**23.9**	**22.4**
520	28.5	26.8	660	23.5	21.9
540	27.6	26.3	680	22.9	21.0
546	**27.4**	**26.1**	700	22.4	20.4

Note: The four wavelengths required by the COM of the IMA are given in bold characters.

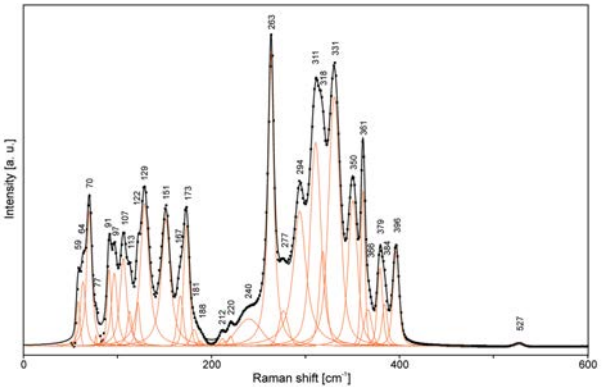

Figure 3. The Raman spectrum of gungerite (excited by 633 nm laser). The experimental spectrum is displayed as a solid black line. The black dotted curve, which matches the black line is a result of a spectral fit as a sum of individual Voigt peaks (orange) shown below the curve.

Si-based charge-coupled device (CCD) detector. After careful tests with different lasers (473, 532, and 633 nm), the 633 nm He-Ne laser with the beam power of 1 mW at the sample surface was selected for spectra acquisition to minimize analytical artifacts. Raman signal was collected in the range of 600–50 cm^{-1} with a 50× objective, and the system operated in the confocal mode; beam diameter was ~2.6 μm and the lateral resolution ~5 μm. Wavenumber calibration was done using the Rayleigh line and low-pressure Ne-discharge lamp emissions. The wavenumber accuracy was ~0.5 cm^{-1}, and the spectral resolution was ~2 cm^{-1}. Band fitting was done after appropriate background correction, assuming combined Lorentzian-Gaussian band shapes using Voigt function (PeakFit; Jandel Scientific Software).

Preliminary assignment of the Raman bands was made by analogy with simple sulfides. Raman bands of As–S stretching vibrations in the Raman spectra of orpiment, As_2S_3, and realgar, AsS, are observed in the range of 360–290 cm^{-1} (Forneris 1969; Minceva-Sukarova et al. 2003). In these minerals, the As-S distances are in the range of 2.21–2.31 Å (Morimoto 1954; Mullen and Nowacki 1972). The largest distances correspond to the lowest frequencies of As–S stretching vibrations. In gungerite, the As–S distances vary from 2.206 to 2.320 Å. Consequently, bands of As–S stretching vibrations are expected to be in the range of 370–280 cm^{-1}.

The band of the highest-intensity Sb–S stretching vibrations in the Raman spectrum of stibnite has been observed within the range of 308–280 cm^{-1} (Mernagh and Trudu 1993; Minceva-Sukarova et al. 2003; Kharbish et al. 2009; Makreski et al. 2014). This corresponds to the band located at 294 cm^{-1} in gungerite. An additional band observed in the Raman spectra of stibnite (in the range 251–236 cm^{-1}) conforms to the shoulder at 240 cm^{-1} in the spectrum of gungerite. This band was assigned to the bending mode of the SbS_3 units (Frost et al. 2010).

A more precise assignment of Raman bands of gungerite can be made based on the comparison with Raman spectra of thallium sulfosalts. In the IR spectrum of lorándite, $TlAsS_2$, bands of As–S stretching vibrations are observed in the range of 380–350 cm^{-1}. The comparison of the Raman spectra of lorándite with the Raman spectra of Sb-bearing thallium sulfosalts containing pyramidal $(As,Sb)S_3$ units (parapierrotite, rebulite, and vrbaite) resulted in the following assignment of Raman bands of SbS_3 units (Makreski et al. 2014; Kharbish 2011): 302–310 cm^{-1} to the asymmetric stretching mode of SbS_3; 334 cm^{-1} to the symmetric stretching mode of SbS_3; 282 and 270 cm^{-1} (weak bands) to the symmetric and asymmetric bending modes of SbS_3, respectively. Consequently, the bands of gungerite observed in the range 400–340 cm^{-1} should be assigned to As–S stretching vibrations, and the bands in the range 340–280 cm^{-1} are due to both As-S and Sb-S stretching vibrations. Noteworthy is that no strong Raman bands are observed in the range 265–250 cm^{-1} of all above-mentioned sulfides and sulfosalts except gungerite.

Based on the estimated As–As bond force constant value of 1.09 mdyn/Å, Muniz-Miranda et al. (1996) assigned the bands at 173 and 184 cm^{-1} in the Raman spectrum of realgar to modes with a significant contribution of As–As stretching. The As–As bond length in realgar is equal to 2.57 Å. For gungerite having a shorter As-As bond (2.4487 Å), a higher frequency of As–As stretching vibrations should be expected.

Unlike other Sb-bearing thallium sulfosalts containing pyramidal $(As,Sb)S_3$ units, gungerite is characterized by the presence of a short As-As bond in the crystal structure and the presence of the strong band at 263 cm^{-1} in the Raman spectrum. Based on this fact, the band at 263 cm^{-1} was assigned to As–As stretching vibrations. This assignment is in good agreement with the Raman spectrum of arsenolamprite (Thomas and Davidson 2010), the strongest Raman band of which is observed at 253 cm^{-1}.

It is to be noted that the As–As bond length in sulfosalts varies over a wide range. For example, in wakabayashilite these bonds are about 2.84 Å long. Correspondingly, no bands in the range of 230–300 cm^{-1} are observed in the Raman spectrum of wakabayashilite (Bindi et al. 2014). A band at 268 cm^{-1} was observed in the Raman spectrum of realgar by Cheng et al. (2017), but the assignment of this band is ambiguous. Moreover, this band was not detected in Raman spectra of realgar in other works. Most probably, the band at 268 cm^{-1} corresponds to pararealgar formed from realgar under laser beam (Muniz-Miranda et al. 1996).

The assignment of Raman bands with wavenumbers below 200 cm^{-1} is ambiguous. Presumably, these bands correspond to soft mixed lattice modes involving As–S–As bending and Tl–S stretching vibrations.

Chemical analysis

Quantitative chemical analyses were carried out using a Cameca SX-100 electron microprobe operated in wavelength-dispersion spectroscopy (WDS) mode applying an accelerating

Table 2. Chemical composition of gungerite based on electron microprobe data

Constituent	wt%	Range	SD	Probe standard
Tl	13.68	13.37–14.13	0.22	Tl(Br,I)
As	26.77	25.32–27.49	0.71	Pararammelsbergite
Sb	30.97	30.45–31.40	0.24	Sb
S	28.02	27.21–28.98	0.60	Chalcopyrite
Total	99.44			

voltage of 25 kV, a beam current of 10 nA and a beam diameter of 1 μm. Analytical data (for 19 points) and standards used are given in Table 2. Contents of other elements with atomic numbers larger than that of carbon were found to be below detection limits. The empirical formula (based on the sum of all atoms = 23 pfu) is $Tl_{0.99}As_{5.29}Sb_{3.77}S_{12.95}$. The ideal chemical formula is $TlAs_5Sb_4S_{13}$, requiring Tl 13.78, As 25.26, Sb 32.85, S 28.11, total 100 wt%.

X-ray crystallography and structure determination

Powder X-ray diffraction

Powder X-ray diffraction data (Table 3) were obtained in Bragg-Brentano geometry using a PANalytical Empyrean powder diffractometer equipped with a Cu X-ray tube and PIXcel3D solid-state detector. A grain of gungerite about 1 mm^3 was placed onto a flat silicon wafer and mildly ground in acetone. The powder X-ray data were collected in the 2θ range 4–80° with a step of 0.013° and an integrated counting time of 200 s per step (accumulation of 40 scans = total data-collection time was ca. 3 days). The unit-cell parameters were refined using the program Celref (Laugier and Bochu 2003). Theoretical *d*-spacings and intensities were calculated from the structure model using the PowderCell program (Kraus and Nolze 1996). The data obtained are affected by an extremely strong preferred orientation effect due to the perfect cleavage of gungerite on (010). Refined orthorhombic unit-cell parameters, obtained from the powder data, are a = 20.18(1) Å, b = 11.528(3) Å, c = 20.14(1) Å, V = 4686(4) $Å^3$ (Z = 8).

Single-crystal X-ray diffraction

For the single-crystal diffraction experiment, a plate-like single-crystal fragment of gungerite, extracted from the polished section, which had been analyzed using an electron microprobe, was selected under a polarized light microscope and mounted on a glass fiber. The diffraction experiment (see Online Materials[1] Table OM1 for details) was performed at room temperature with a Rigaku SuperNova single-crystal diffractometer equipped with the Atlas S2 CCD detector and a microfocus Mo$K\alpha$ source. Data reduction was performed using CrysAlisPro Version 1.171.39.46 (Rigaku 2019). The data were corrected for Lorentz factor, polarization effect, and absorption (multi-scan, ABSPACK scaling algorithm; Rigaku 2019). According to the single-crystal X-ray data, gungerite is orthorhombic, with the space group *Pbcn*. The unit-cell parameters determined from the single-crystal data are as follows: a = 20.1958(3) Å, b = 11.5258(2) Å, c = 20.1430(2) Å, V = 4688.74(12) $Å^3$ (Z = 8). The apparent pseudotetragonality of the [010] direction (Figs. 4a and 4b) expresses the large-scale geometry of the structure but is not supported by structure details. In this respect the structure reminds one of the structure of lorándite $TlAsS_2$ (Balić-Žunić et al. 1995) in which, however, distortions away from pseudotetragonality are more pronounced.

Table 3. Powder X-ray diffraction data for gungerite (the d_{hkl} spacings are given in angstroms)

I_{rel} (%)	d_{obs}	d_{calc}	I_{calc}	h	k	l
1	10.047	10.083	23	2	0	0
3	8.957	8.985	22	1	1	1
1	7.153	7.122	3	2	0	2
100	5.755	5.759	68	0	2	0
1	5.593	5.578	20	3	1	1
1	5.337	5.339	8	1	2	1
1	5.026	5.041	8	4	0	0
1	4.844	4.851	<1	1	2	2
2	4.479	4.478	60	2	2	2
4	4.273	4.274	28	3	2	1
		4.270	24	1	2	3
6	3.705	3.707	37	1	3	1
1	3.661	3.663	100	3	2	3
1	3.564	3.549	18	4	2	2
		3.546	21	2	2	4
2	3.379	3.380	32	2	3	2
1	3.342	3.366	50	6	0	0
		3.353	48	0	0	6
1	3.311	3.310	10	5	1	3
1	3.329	3.289	6	3	3	1
1	3.070	3.072	31	6	1	2
10	3.030	3.029	23	4	2	4
10	2.901	2.903	27	6	2	0
14	2.878	2.880	15	0	4	0
5	2.850	2.851	3	0	4	1
10	2.821	2.822	42	1	4	1
1	2.769	2.768	3	0	4	2
		2.763	20	1	1	7
1	2.670	2.670	22	2	4	2
1	2.624	2.624	3	1	4	3
1	2.557	2.556	27	7	2	1
1	2.504	2.500	5	7	0	4
1	2.289	2.286	14	1	3	7
2	2.274	2.274	12	1	5	1
1	2.248	2.247	9	2	2	8
1	2.236	2.239	2	4	4	4
		2.232	1	2	5	1
1	2.212	2.211	7	3	4	5
1	2.191	2.195	15	6	2	6
1	2.128	2.124	1	5	4	4
1	2.092	2.096	2	8	3	1
1	1.780	1.780	17	8	0	8
1	1.727	1.727	11	5	6	1
1	1.425	1.424	3	10	0	10

The crystal structure of gungerite was solved from the single-crystal X-ray data using intrinsic-phasing with the SHELXT program (Sheldrick 2015) and refined by the software Jana2006 (Petříček et al. 2014). The structure is strongly pseudo-tetragonal, and during the import into Jana2006 the twinning due to the metric merohedry (diffraction type I; Petříček et al. 2016) was introduced as it is possible within the space-group test in Jana2006. Subsequent refinement returned reasonable fractions of the twin domains and resulted in excellent final R-values (Online Materials[1] Table OM1). Anisotropic displacement parameters were refined for all atoms. Except for the higher average displacement parameter of Tl, which is in agreement with its low-charge and large interatomic Tl-S distances, and with the special way in which Tl is inserted in the structure (specified below), this structure is distinguished by fairly uniform and evenly distributed atomic displacement values for all atoms. The atom coordinates, atomic displacement parameters, and site occupancies are given in Online Materials[1] Table OM2 and selected interatomic distances in Table 4.

Description of the structure

The crystal structure of gungerite is undoubtedly the most complex among all new sulfosalts discovered at the deposit. It

contains 23 atomic sites, one site occupied purely by Tl, one site purely by Sb, three sites purely by As, three Sb-dominant sites, and two As-dominant sites that are mixed-occupied. The sites with mixed occupancies are as follows: Sb2 [0.840(12) Sb/0.160(12) As], Sb3 [0.844(13)Sb/0.156(13) As], Sb4 [0.781(11)Sb/0.219(11) As], As1 [0.820(12) As/0.180(12)Sb], and As2 [0.938(12) As/0.062(12)]. The crystal structure consists of (As,Sb)–S clusters, which have van der Waals contacts to most of the surroundings, and otherwise are connected to them only by sparse metal cation–sulfur bonds. These clusters have a peculiar arrangement, being "stacked" on, around, and along Tl–S rods parallel to [010]. An individual cluster, always doughnut-shaped (or toroid-shaped), has a central Tl polyhedron half-inserted into it. The cluster is formed by a chelating mirror-symmetrical group ("almost a molecule"), which has Sb-As "defect coordination cubes" as forceps (with some atoms missing from a perfect cube-model). Its two mirror-related arms are connected by the coordination pyramid of As3 (Fig. 5). One arm of the chelating group has an eyelet of doubly interconnected Sb1 and Sb3 as its terminal portion. Through the coordination pyramid of As1, the eyelet is connected to the centrally positioned pyramid of As3, from which starts the other arm of the chelating group. In the order of appearance, this arm consists of the coordination pyramid of As2 and a terminal eyelet of Sb2 and Sb4. These two Sb atoms are doubly interconnected via two sulfurs. A radially oriented "tail-group" points out of the cluster and is formed by a covalent As-As bond (2.448 Å long), which connects As3 with As4. After the As4 polyhedron (which still is in a mirror-symmetric position with the rest of the "molecule") As5 follows, which points sideways, counter to the *m* symmetry of the group. However, an As5 polyhedron from an adjacent "molecule" is a mirror-symmetrical "plug" that closes the doughnut body from the side, which was left open by the original group (Fig. 5).

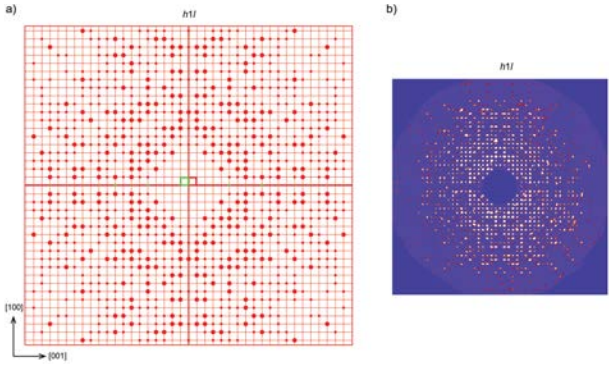

Figure 4. Pseudotetragonal single-crystal X-ray diffraction pattern of gungerite. (**a**) Simulated *h1l* layer of the reciprocal space of gungerite. Reflections from the two domains overlap completely (except of the few reflections on the zero rows) due to twinning by metric merohedry. Two twin domains of the gungerite unit cell are displayed as red and green squares. (**b**) Reciprocal space reconstruction (*UNWARP* tool) of the *h1l* layer from the experimental X-ray data. Simulation done from the refinement reflection file in Jana2006. The radii of the reflections are scaled by their intensities.

Table 4. Selected interatomic distances (in angstroms) for gungerite

Tl1–S2	3.528(2)	As1–S2	2.317(4)
Tl1–S3^{i}	3.453(2)	As1–S9	2.295(4)
Tl1–S4	3.150(4)	As1–S13	2.320(2)
Tl1–S5	3.190(2)		
Tl1–S8	3.452(2)	As2–S8	2.287(3)
Tl1–S9	3.373(4)	As2–S10	2.303(2)
Tl1–S9^{iii}	3.526(4)	As2–S11	2.289(4)
Tl1–S11	3.514(4)		
Tl1–S11^{iii}	3.470(4)	As3–S10	2.263(4)
		As3–S13	2.256(4)
Sb1–S1	2.610(3)		
Sb1–S2	2.488(2)	As3–As4	2.4487(17)
Sb1–S3^{ii}	2.921(2)		
Sb1–S5	2.497(2)	As4–S6	2.250(4)
		As4–S7^{xii}	2.250(4)
Sb2–S4	2.411(4)	As4–S10	3.200(3)
Sb2–S11	2.466(4)		
Sb2–S12	2.506(2)	As5–S3	2.206(2)
		As5–S6	2.294(4)
Sb3–S1	2.464(2)	As5–S7	2.295(4)
Sb3–S5	2.436(3)		
Sb3–S9	2.473(4)		
Sb4–S4	2.497(2)		
Sb4–S8	2.466(2)		
Sb4–S12	2.429(2)		

Symmetry codes: (1) $-x + 1/2, -y + 1/2, z + 1/2$; (2) $x, -y, z + 1/2$; (3) $-x + 1/2, y - 1/2, z$; (12) $-x + 1, y, -z + 1/2$.

The coordination polyhedron of Tl is inserted in the cavity of the doughnut, and shares S atoms with the As/Sb coordination polyhedra (Figs. 5 to 7). The coordination number of Tl is nine. Among the bonds formed by Tl, six have lengths below 3.5 Å and three more are shorter than 3.6 Å. When all distances below 4.2 Å are included, the total is 11 Tl-S distances. Most remarkable are two short distances, 3.150 Å to S4 and 3.190 Å to S5, and a short Tl1-As3 bond having the length of 3.403 Å, well within the range of Tl-S distances (Table 4). The polyhedron shape is irregular, with three tetragon-shaped faces approximating a part of a distorted cube (Fig. 6). Thallium is embedded in one (010) face of the doughnut cluster, whereas S9 and S11 are a part of the surface opposite to it. Their 90°-rotated opposites, S9 and S11, are already a part of the adjacent cluster (Fig. 6). The sulfur sites S2, S3, S4, S5, and S8 surround Tl in the Tl-centered cluster. The faces of the Tl-centered polyhedron are as follows:

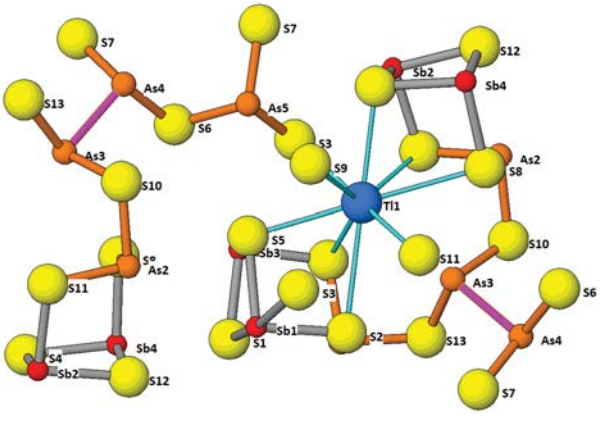

Figure 5. Chelating As/Sb group, inserted thallium atom and an As5 "plug" from another group, form together a unit-cluster of the gungerite structure. In all figures, large yellow spheres are S, large blue spheres Tl, red spheres (gray strong bonds) are Sb, and brown spheres (brown strong bonds) are As. Covalent As-As bonds displayed in mauve.

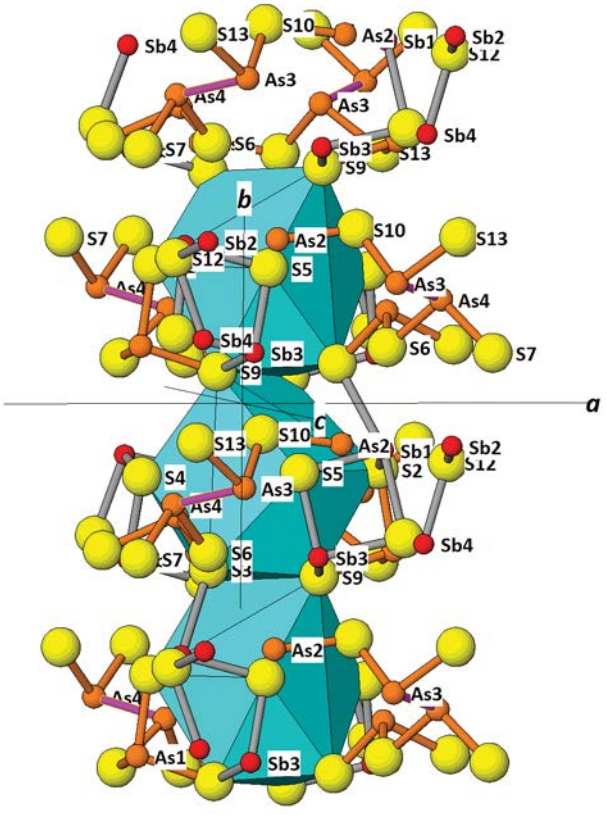

Figure 6. Four clusters ("doughnuts") formed by concatenated As- and Sb-coordination pyramids, strung along a rod of coordination polyhedra of thallium (in azure).

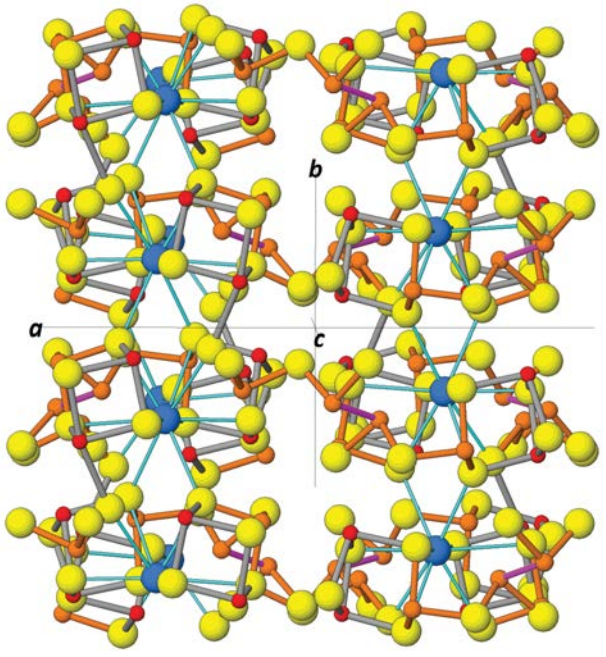

Figure 7. Two chains consisting of thallium (blue) with the attached clusters formed by As- and Sb-pyramids. Correlation between cluster orientations results in column interconnections as illustrated.

broken tetragons S4-S8-S9-S11, S2-S5-S9-S11, and S3-S4-S9-S5; irregularly broken pentagons S3-S4-S11-S9-S5 and S2-S9-S11-S8-S11; conspicuous triangles S2-S5-S9 and S4-S8-S11.

The As3 atom close to Tl, acts as a cap of the broad pentagon S2-S9-S11-S8-S11, which encircles a sulfur-free side of the Tl coordination polyhedron. It can represent the interaction of the lone electron pairs of Tl and As, opposed to the short bonds from Tl to S4, S5, and S9. The short Tl-As distance is analogous to those found in gabrielite, $Tl_2AgCu_2As_3S_7$ (3.11 Å), erniggliite, $Tl_2SnAs_2S_6$ (3.259 Å), richardsollyite, $TlPbAsS_3$ (3.397 Å), arsiccioite, $AgHg_2TlAs_2S_6$ (from 3.397 Å), and in several Tl sulfosalts with distances about and above 3.48 Å (summarized by Makovicky 2018). Thus, gungerite is one more example of cation-cation interactions, again with demonstrable involvement of lone electron pairs of both cations. Coordination polyhedra of thallium are interconnected and form "rods" via sharing the S9-S11 joins (Fig. 6). These joins alternate their orientation by about 90° along the "rod" of Tl-centered polyhedra, which runs parallel to [010]. Although they necessarily are "soft," these rods and the As-Sb clusters centered on them represent the substance of the gungerite structure (Figs. 6 and 7).

The short covalent As3-As4 bond, which is 2.448 Å long (Figs. 5 and 8), is analogous to such bonds in the small molecules, which are present in the structures of realgar, AsS (2.57 Å), alacranite, As_8S_9 (2.62 Å), pararealgar, As_4S_4 (2.48 and 2.53 Å),

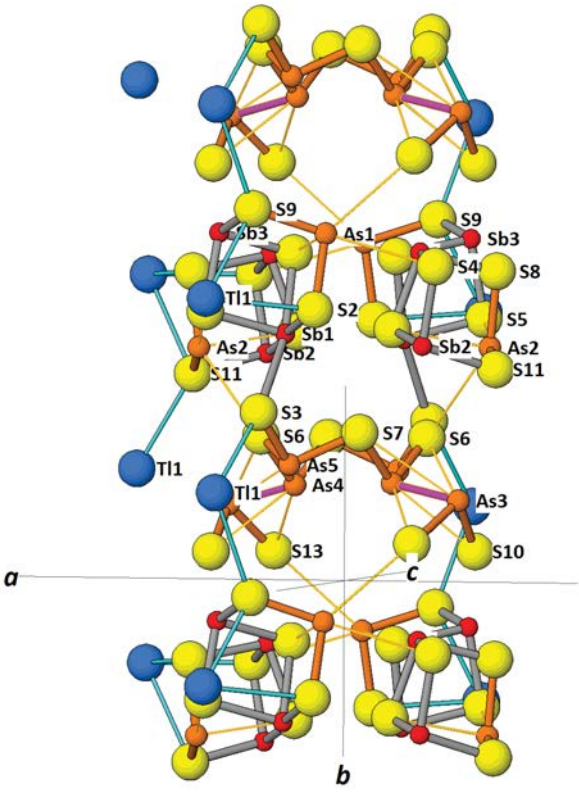

Figure 8. Interconnection of four adjacent "rod-and-cluster" columns across the interspace. The drawing contains corner configurations from four columns and the corresponding bridging atoms and bonds. Thin lines (in gold) describe long cation-anion interactions.

dimorphite, As_4S_3 (2.44 Å), and uzonite, As_4S_5 (2.55 Å) (summarized by Makovicky 2006). Except for uzonite, these molecules have two covalent As-As bonds each; only in the structure of realgar these bonds are distributed over different pairs of As atoms, whereas they are restricted to one As atom in the rest.

The coordination polyhedron of As3 is a pentagonal pyramid with two short bonds and three long distances in the base; the vertex is occupied by the arsenic atom As4. Besides two short As-S bonds (2.249 Å), As4 has two shorter weak bonds, 3.199 Å to S10 and 3.226 Å to S13 (which, remarkably, also coordinate the As3 atom); the remaining As-S distances are longer than 4.17 Å. The shortest As-As contacts are 3.392 and 3.411 Å to As5, and 3.504 Å to directly opposing As4 in the As4-As5-As4-As5 ring. The Sb3 atom has a pentagonal pyramidal coordination, with short bonds to S1 and S9, and three long distances to S8, S6, and S3. The As2 atom has a broad trapezoidal coordination, being bonded to S10 and S11, and has long distances to S5 and S12. The pentagonal coordination of As5 is based on short bonds to S6 and S7, long distances to S4 and S5, and this trapezoidal arrangement is completed by a long contact to Tl1 (4.141 Å). We can see that the activity of the lone electron pairs of arsenic is much less constrained in gungerite than, e.g., in orpiment.

The complex structure of gungerite makes a distinct imprint on the distribution of bonding and non-bonding distances. When we concentrate on the interdependence and counter-play of short strong As/Sb bonds and of the long distances generally opposing them, these pairs of distances concentrate around the values of 2.45 vs. 3.40 Å for the mixed Sb/As sites (where Sb prevails), whereas around 2.25–2.30 Å vs. 3.40 Å for the (mostly mixed) As/Sb sites (where As prevails). The As3-As4 pair of covalently bonded arsenic atoms (As-As 2.449 Å) has opposing distances at or above 3.8 Å. The As5 site has all the long distances at and above 3.65 Å, and one distant ligand (out of three) actually is missing.

Concerning the [010] stacking of clusters ("molecules") on an individual Tl rod, the consecutive clusters are related by the (100) *b*-glide, i.e., the orientation of As-As bond in them alternates, comprising ~90° to one another in the (010) projection. In the stacking along the rod, the Sb-based group of the chelate always separates two consecutive As3-As4 groups, which have the same orientation in a stack of clusters around the Tl rod. For adjacent columns (Tl rods), which are arrayed along the *a*-axis, these configurations are related by inversion and they "face" the opposite [00±1] directions (Fig. 9).

Interconnection of clusters and rods

Those clusters, which are attached to one thallium rod, face one another by their lone electron pairs and are connected only by one medium-strong Sb1-S3 bond (Fig. 6). The Sb1 cation has two strong bonds to sulfur inside its cluster (2.488 Å to S2 and 2.496 to S5), whereas the third short bond to S1 is stretched, 2.611 Å, and is opposed by the shortest weaker interaction of 2.921 Å to the next cluster. The remaining long interactions of the Sb1 cluster measure 3.262 and 3.701 Å; they are oriented to S12 in different "molecules." In the (pseudo)mirror-symmetrical position Sb4, the analogous short bond is Sb4–S12, and it is 2.430 Å long.

Outer surfaces of the approximately square-shaped clusters are full of outward-radiating lone electron pairs of Sb and/or As. The strong-bond connection takes place only at their corners, via As4-S7/S6-As5 connections, bent via the covalent As4-S7/S6 and S7/S6-As5 bonds (Figs. 8 and 9). Always, two opposing corners of the cluster have trigonal pyramids of As5 with two arms pointing into the meeting space of four columns. They are joined by two As4 atoms via common S6/S7 sites. The As4 sites are stabilized by the As3-As4 bonds. All four As atoms in the elongate hexagon-shaped As4-As5-As4-As5 group have lone electron pairs approximately oriented in the same direction. Because of the internal glide plane in each column, this connection occurs in one column only in every second cluster, and the contacts of intervening clusters occur via weak contacts of As1 polyhedra (Fig. 8). This situation involving both high force and weak interactions may lead to high-frequency vibrations and to displacements that contribute to the low-energy vibrations documented by Raman spectroscopy.

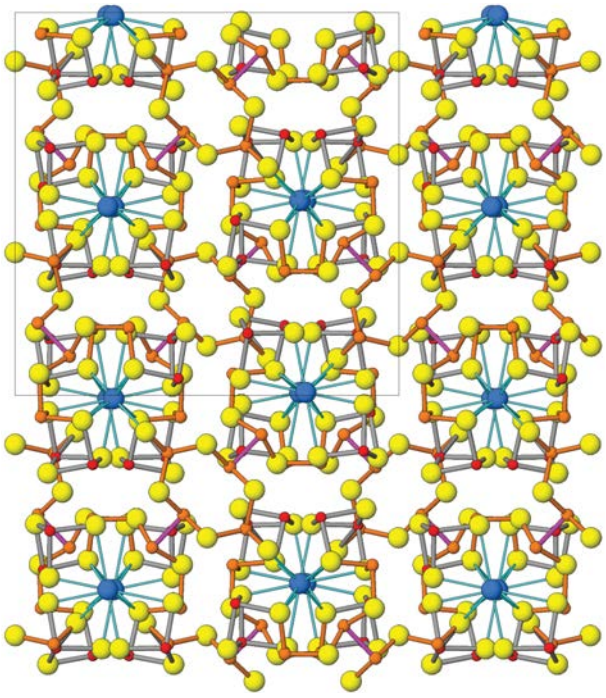

Figure 9. Crystal structure of gungerite projected along [010]. In the drawing, the ***a*** axis is horizontal, ***c*** axis is vertical. The space in between the rods is filled with lone-electron pairs of Sb and As.

Discussion

Related structures

With its pseudo-tetragonal character (Fig. 9) and low content of thallium, the crystal structure of gungerite is unique among Tl-As sulfosalts. Interesting analogies on a more local scale were found between gungerite and gillulyite, $Tl_2(As,Sb)_8S_{13}$ (Foit et al. 1995; revised by Makovicky and Balić-Žunić 1999). The latter structure has the *b* parameter equal to 5.679 Å, i.e., one half of the *b* parameter of gungerite. It can be interpreted as broad double-ribbons, which form tightly bonded SnS-like layers, stacked and separated by lone electron pairs micelles (spaces).

Some arsenic polyhedra complicate this scheme, being oriented diagonally to the orientation of the majority of polyhedra. This somewhat resembles the As-Sb clusters and their spacing in gungerite along the Tl rods.

As one can see in the projection along the *b* axis (Fig. 9), the structure of gillulyite consists of periodically constricted (001) layers separated by spaces with lone electron pairs and long weak interactions. The periodically constricted layer can be understood as stacking of diagonally oriented ellipsoidal arrangements of eight cation sites [occupied by (As, Sb), only the apical ones with Tl-and-(As,Sb) alternation] (Fig. 10). Short cation-sulfur bonds are oriented inward, and the mostly weak, long cation–sulfur distances outward. This was the pattern also recognized in the Patterson map of gungerite, in which the apices of the ellipses are occupied by thallium, and the six remaining cation sites alternatively by As and Sb (Fig. 10). The corresponding pattern of short bonds and S positions in gungerite partly (but not fully) resembles that seen in gillulyite. The principal difference is that in gillulyite this ellipsoidal configuration is centered above split Tl positions, whereas in our case there are Sb/As atoms below it, close to the *foci* of the projected ellipse. It was recognized that they form part of another complete ellipse below the first one, oriented at ~90° to the first one (Fig. 11).

In gungerite, every thallium site forms a part of the [101] string of such ellipsoidal configurations, which have the same overall *y* parameter (Fig. 11). This string runs diagonally to the unit cell axes, as does another string, at 90° to the first one, and with a different *y* parameter. Parallel strings alternatively assume two *y* levels, ½ *b* apart. Another such system of strings runs parallel to the other diagonal. In its totality, this remarkable system of superimposed ellipsoidal arrangements appears to make maximum space for the lone electron pair configurations of As and Sb, especially in the channels, which are created by overlapping ellipses (Fig. 11).

The other thallium-arsenic sulfosalt, which has a columnar structure is lorándite, $TlAsS_2$ (Zemann and Zemann 1959; Fleet 1973; Balić-Žunić et al. 1995). It is situated practically at the opposite pole of the Tl:(As,Sb) spectrum of compositions. In this monoclinic structure, rods are much thinner, each formed by a spiral of As-S coordinations, with the As atoms on the edges of square-shaped rods and with the long interactions (3.953 Å and longer) interconnecting the rods. Tl atoms alternate with the As atoms along the rod edges and Tl-S distances participate in the *rod-to-rod* bonding, unlike those in gungerite.

Twinning

As mentioned above, twinning is present in the investigated crystal, with the twinning matrix (00$\bar{1}$/010/100) and the two twin fractions 0.8354(9)/0.1646(9). The simplest twinning model assumes the [010] rods intact, with their internally active *b* glide plane and the chessboard scheme of alternating [010] and [0$\bar{1}$0] orientations preserved (Fig. 12). One of the (001) rod walls is broader and slightly convex, and it faces the opposite (001) wall of the next rod, which is narrower and slightly concave. As a consequence, the (100) walls are slightly convergent (Fig. 11), and they meet with the like walls of adjacent rods along *a* direction. The rods are interconnected by strong bonds only rarely, in places where four of them meet (Figs. 7 and 11); all

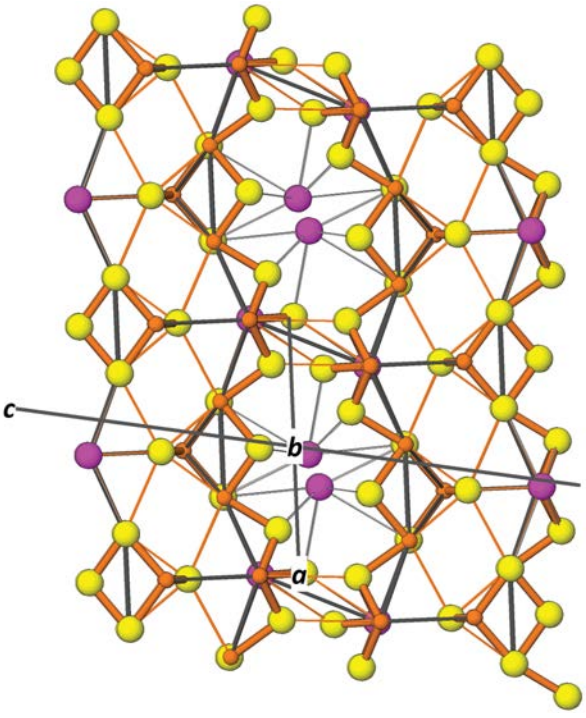

Figure 10. Elliptical arrangement of As, Sb and apical (Tl, Sb) atoms in one (010) slab of the crystal structure of gillulyite. The inclined ellipses are tightly packed and share some cations. They are underlain by split Tl sites, unlike those in gungerite.

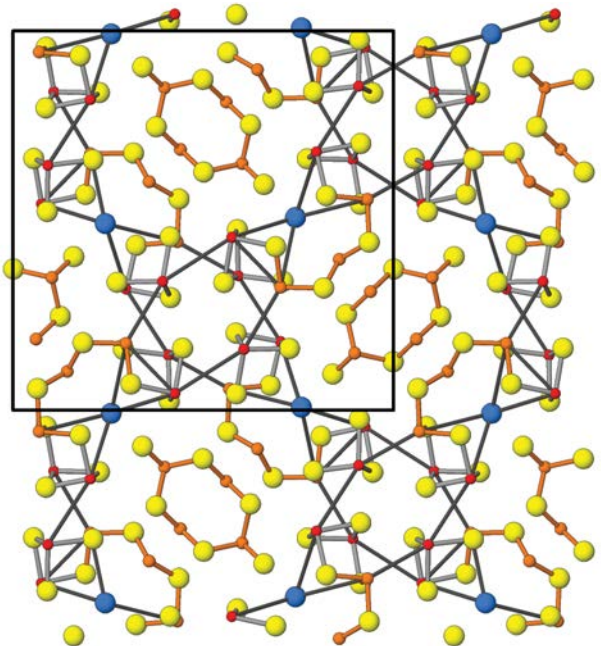

Figure 11. Elliptical arrangement of As, Sb, and apical Tl atoms in one (010) slab of "doughnut" clusters in gungerite. Configurations between the intersecting rows of ellipses represent compressed As4-As5-As4-As5 rings and covalently bonded As3-As4 pairs. Alternative diagonal strings of ellipses are positioned halfway between the indicated ones, on the other (010) level of clusters, 0.5 b apart.

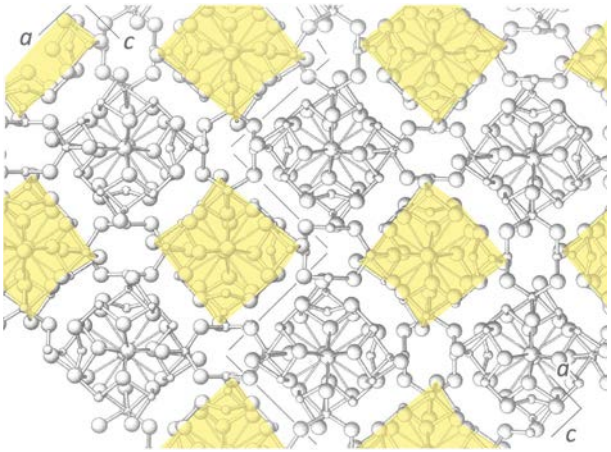

Figure 12. Visualization of twinning in the crystal structure of gungerite. The composition "plane" is represented here by a zigzag contact via long-range interactions instead of a hypothetical "planar" contact. The [010] and [0$\bar{1}$0] oriented rods are distinguished by coloring, forming a chessboard pattern in both domains. Axis orientation is indicated for both domains.

other interspaces between the rods are filled by lone electron pairs and van der Waals contacts.

The observed twinning can tentatively be connected with the As-Sb interchange, detected in the majority of cation positions (specified above). Except for Sb1, which interconnects adjacent doughnuts in a rod (unlike its counterpart, Sb4, which is without such interconnection), the pure, unmixed cation sites are situated on rod corners, and not in its walls. Interchange of cations in the latter, wall positions, where they have long-range interactions with opposing rods, might favor the changes connected with twinning. The approximate equality between the volume ratios of twin domains and those of cation ratios in the (As,Sb)1, (As,Sb)2, (Sb,As)2, and (Sb,As)3 positions is strongly suggestive of such connection.

On the structure level, twinning is represented by a twofold screw axis parallel to [101] with a shift of the only ¼ of the full [101] repetition period (Dornberger-Schiff designation $2_{1/2}$; Dornberger-Schiff 1966) instead of ½ of the repetition period (designation 2_1) of the usual screw axis. As a result, the given twinning operation is an order-disorder (OD) operation and two positions of the twinned domain are possible, either produced by the $2_{1/2}$ operation or by $2_{-1/2}$. They become identical on the macrocrystal scale.

On the macrocrystal level, the twin law (00$\bar{1}$/010/100), also is a matrix for a fourfold twin law with the rotation axis parallel to [010]. Close inspection of the twinned structure, however, shows that the crystal structure orientation after two partial 90° rotations is identical to the initial one, except for a small shift of the $a/2+c/2$ size, which is invisible on a macrocrystal. This means that the twin consists of two and not four individuals (crystal orientations), and the twin law is a dichroic fourfold inversion axis, –4, without additional twofold axes perpendicular to it. It also should be mentioned that there are two categories of twin operation descriptions, one classical, on a macrocrystal level, and another, perhaps non-classical, but describing exactly what happens during twinning on the composition plane; both are given here.

Implications

The crystal structure of gungerite appears to be unique among the structures of Tl-As-Sb sulfides. As a remarkable case of inorganic structural architecture, "doughnuts," that display imperfect reflection symmetry in the gungerite structure are organized into semi-independent *polar* rods with a glide-plane symmetry; these, in turn, are arranged in a chessboard pattern of [010] and [0$\bar{1}$0] rods via two additional systems of glide planes, twofold axes, and inversion centers of the *Pbcn* group. The profusion of van der Waals interactions and the presence of sparse covalent interconnections at critical points of the structure make it an interesting object of future structural dynamics studies.

Acknowledgments and Funding

Three anonymous reviewers and Associate Editor Diego Gatta are thanked for constructive comments, which improved the manuscript. The friendly interest of T. Balić-Žunić and further colleagues involved in the studies of arsenic-rich Tl mineralizations is acknowledged with pleasure. We acknowledge Czech-NanoLab Research Infrastructure supported by MEYS CR (LM2018110) for the financial support of the measurements. The interpretation of the Raman spectrum was performed in accordance with the state task, state registration No. AAAA-A19-119092390076-7.

References cited

Balić-Žunić, T., Makovicky, E., and Moëlo, Y. (1995) Contributions to the crystal chemistry of thallium sulphosalts. III. The crystal structure of lorandite ($TlAsS_2$) and its relation to weissbergite ($TlSbS_2$). Neues Jahrbuch für Mineralogie—Abhandlungen, 168, 213–235.

Bindi, L., Bonazzi, P., Zoppi, M., and Spry, P.G. (2014) Chemical variability in wakabayashilite: A real feature or an analytical artifact? Mineralogical Magazine, 78, 693–702.

Cheng, H., Zhou, Y., and Frost, R.L. (2017) Structure comparison of orpiment and realgar by Raman spectroscopy. Spectroscopy Letters, 50, 23–29.

Dornberger-Schiff, K. (1966) Lehrgang über OD-Strukturen. Akademie-Verlag.

Fleet, M.E. (1973) The crystal structure and bonding of lorándite. Zeitschrift für Kristallographie, 138, 147–160.

Foit, F.F., Jr., Robinson, P.D., and Wilson, J.R. (1995) The crystal structure of gillulyite, $Tl_2(As,Sb)_8S_{13}$ from the Mercur gold deposit, Tooele. County, Utah, U.S.A. American Mineralogist, 80, 394–399.

Forneris, R. (1969) Infrared and Raman spectra of realgar and orpiment. American Mineralogist, 54, 1062–1074.

Frost, R.L., Bahfenne, S., and Keeffe, E.C. (2010) Raman spectroscopic study of the mineral gerstleyite $Na_2(Sb,As)_8S_{13}\cdot 2H_2O$ and comparison with some heavy-metal sulfides. Journal of Raman Spectroscopy, 41, 1779–1783.

Gresham, C., and Lawrey, E.A. (2018) Thallium Toxicity. Medscape; https://emedicine.medscape.com/article/821465-overview.

Ikramuddin, M. (1985) Thallium in various types of gold deposits. Conference: 98th annual meeting of the Geological Society of America, Orlando, Florida, U.S.A., 28 Oct 1985, Geological Society of America, Abstr. Programs, vol. 17.

Karbowska, B. (2016) Presence of thallium in the environment: sources of contaminations, distribution and monitoring methods. Environmental Monitoring and Assessment, 188, 640.

Kasatkin, A.V., Nestola, F., Agakhanov, A.A., Škoda, R., Karpenko, V.Y., Tsyganko, M.V., and Plášil, J. (2018a) Vorontsovite, $(Hg_5Cu)_{\Sigma 6}TlAs_4S_{12}$, and ferrovorontsovite, $(Fe_5Cu)_{\Sigma 6}TlAs_4S_{12}$: The Tl- and Tl-Fe-analogues of galkhaite from the Vorontsovskoe gold deposit, Northern Urals, Russia. Minerals, 8, 185.

Kasatkin, A.V., Makovicky, E., Plášil, J., Škoda, R., Agakhanov, A.A., Karpenko, V.Y., and Nestola, F. (2018b) Tsygankoite, $Mn_8Tl_8Hg_2(Sb_{21}Pb_2Tl)\Sigma_{24}S_{48}$, a new sulfosalt from the Vorontsovskoe gold deposit, Northern Urals, Russia. Minerals, 8, 218.

Kasatkin, A.V., Makovicky, E., Plášil, J., Škoda, R., Chukanov, N., Stepanov, S., Agakhanov, A.A., and Nestola, F. (2019) Gladkovskyite, $MnTlAs_3S_6$, a new thallium sulfosalt from the Vorontsovskoe gold deposit, Northern Urals, Russia. Journal of Geosciences, 64, 207–218.

Kasatkin, A.V., Makovicky, E., Plášil, J., Škoda, R., Agakhanov, A.A., Stepanov, S.Y., and Palamarchuk, R.S. (2020) Luboržákite, Mn_2AsSbS_5, a new member of pavonite homologous series from Vorontsovskoe gold deposit. Mineralogical Magazine, 84, 738–745.

Kasatkin, A.V., Stepanov, S.Y., Tsyganko, M.V., Škoda, R., Nestola, F., Plášil, J.,

Makovicky, E., Agakhanov, A.A., and Palamarchuk, R.S. (2022a) Mineralogy of the Vorontsovskoe gold deposit (Northern Urals). Mineralogy, 8(1), 5–93.
Kasatkin, A.V., Plášil, J., Makovicky, E., Škoda, R., Agakhanov, A.A., and Tsyganko, M.V. (2022b) Pokhodyashinite, $CuTlSb_2(Sb_{1-x}Tl_x)AsS_{7-x}$, a new thallium sulfosalt from the Vorontsovskoe gold deposit, Northern Urals, Russia. Journal of Geosciences, 67, in press, DOI: 10.3190/jgeosci.342.
Kasatkin, A.V., Plášil, J., Makovicky, E., Chukanov, N.V., Škoda, R., Agakhanov, A.A., Stepanov, S.Y., and Palamarchuk, R.S. (2021) Auerbakhite, $MnTl_2As_2S_5$, a new thallium sulfosalt from the Vorontsovskoe gold deposit, Northern Urals, Russia. Journal of Geosciences, 66, 89–96.
Kharbish, S. (2011) Raman spectroscopic investigations of some Tl-sulfosalt minerals containing pyramidal (As,Sb)S_3 groups. American Mineralogist, 96, 609–616.
Kharbish, S., Libowitzky, E., and Beran, A. (2009) Raman spectra of isolated and interconnected pyramidal XS_3 groups (X = Sb, Bi) in stibnite, bismuthinite, kermesite, stephanite and bournonite. European Journal of Mineralogy, 21, 325–333.
Kraus, W., and Nolze, G. (1996) POWDER CELL—A program for the representation and manipulation of crystal structures and calculation of the resulting X-ray powder patterns. Journal of Applied Crystallography, 29, 301–303.
Laugier, J., and Bochu, B. (2003) CELREF: Unit-Cell Refinement Program from Powder Diffraction Diagram. Laboratoires des Matériaux et du Génie Physique, Ecole Nationale Supérieure de Physique de Grenoble (INPG), Grenoble, France.
Makovicky, E. (2006) Crystal structures of sulfides and other chalcogenides. Reviews in Mineralogy and Geochemistry, 61, 7–125.
——— (2018) Modular crystal chemistry of thallium sulfosalts. Minerals, 8, 478
Makovicky, E., and Balić-Žunić, T. (1999) Gillulyite $Tl_2(As,Sb)_8S_{13}$: Reinterpretation of the crystal structure and order-disorder phenomena. American Mineralogist, 84, 400–406.
Makreski, P., Jovanovski, G., and Boev, B. (2014) Micro-Raman spectra of extremely rare and endemic Tl-sulfosalts from Allchar deposit. Journal of Raman Spectroscopy, 45, 610–617.
Mernagh, T.P., and Trudu, A.G. (1993) A laser Raman microprobe study of some geologically important sulphide minerals. Chemical Geology, 103, 113–127.
Minceva-Sukarova, B., Jovanovski, G., Makreski, P., Soptrajanov, B., Griffith, W., Willis, R., and Grzetic, I. (2003) Vibrational spectra of $M^{I}M^{III}S_2$ type synthetic minerals (M^{I} = Tl or Ag and M^{III} = As or Sb). Journal of Molecular Structure, 651-653, 181–189.
Morimoto, N. (1954) The crystal structure of orpiment. Mineralogical Journal, 1, 160–169.
Mullen, D.J.E., and Nowacki, W. (1972) Refinement of the crystal structures of realgar, AsS and orpiment, As_2S_3. Zeitschrift für Kristallographie, 136, 48–65.
Muniz-Miranda, M., Sbrana, G., Bonazzi, P., Menchetti, S., and Pratesi, G. (1996) Spectroscopic investigation and normal mode analysis of As_4S_4 polymorphs. Spectrochimica Acta Part A: Molecular and Biomolecular Spectroscopy, 52, 1391–1401.
Murzin, V.V., Naumov, E.A., Azovskova, O.B., Varlamov, D.A., Rovnushkin, M.Y., and Pirajno, F. (2017) The Vorontsovskoe Au-Hg-As ore deposit (Northern Urals, Russia): Geological setting, ore mineralogy, geochemistry, geochronology and genetic model. Ore Geology Reviews, 85, 271–298.
Petříček, V., Dušek, M., and Palatinus, L. (2014) Crystallographic computing system Jana2006: General features. Zeitschrift Für Kristallographie—Crystalline Materials, 229, 345–352.
Petříček, V., Dušek, M., and Plášil, J. (2016) Crystallographic computing system Jana2006: Solution and refinement of twinned structures. Zeitschrift für Kristallographie—Crystalline Materials, 231, 583–599.
Rigaku (2019) CrysAlis CCD and CrysAlis RED. Rigaku-Oxford Diffraction Ltd.
Sazonov, V.N., Murzin, V.V., and Grigor'ev, N.A. (1998) Vorontsovsk gold deposit: An example of carlin-type mineralization in the urals. Russia. Geology of Ore Deposits, 40, 139–151.
Sheldrick, G.M. (2015) SHELXT—Integrated space-group and crystal-structure determination. Acta Crystallographica. Section A, Foundations and Advances, 71, 3–8.
Thomas, R., and Davidson, P. (2010) Hambergite-rich melt inclusions in morganite crystals from the Muiane pegmatite, Mozambique and some remarks on the paragenesis of hambergite. Mineralogy and Petrology, 100, 227–239.
Turekian, K.K., and Wedepohl, K.H. (1961) Distribution of the Elements in some major units of the Earth's crust. Geological Society of America. Bulletin, 72, 175–192.
Vikentyev, I.V., Tyukova, E.E., Murzin, V.V., Vikent'eva, O.V., and Pavlov, L.G. (2016) Vorontsovsk gold deposit. Geology, gold modes, genesis, 204 p. Fort Dialog-Iset (in Russian).
Zemann, A., and Zemann, J. (1959) Zur Kenntnis der Kristallstruktur von Lorandit, $TlAsS_2$. Acta Crystallographica, 12, 1002–1006.

Manuscript received February 2, 2021
Manuscript accepted May 27, 2021
Manuscript handled by G. Diego Gatta

Endnote:

[1]Deposit item AM-22-68003, Online Materials. Deposit items are free to all readers and found on the MSA website, via the specific issue's Table of Contents (go to http://www.minsocam.org/MSA/AmMin/TOC/2022/Jun2022_data/Jun2022_data.html). The CIF has been peer reviewed by our Technical Editors.